Universiteit
Antwerpen

This item is the archived peer-reviewed author-version of:

Electronic properties of 2H-stacking bilayer MoS_2 measured by terahertz time-domain spectroscopy

Reference:
Cheng Xingjia, Xu Wen, Wen Hua, Zhang Jing, Zhang Heng, Li Haowen, Peeters François, Chen Qingqing.- Electronic properties of 2H-stacking bilayer MoS_2 measured by terahertz time-domain spectroscopy
Frontiers of physics - ISSN 2095-0470 - 18:5(2023), 53303
Full text (Publisher's DOI): https://doi.org/10.1007/S11467-023-1295-1
To cite this reference: https://hdl.handle.net/10067/1973980151162165141

uantwerpen.be
Institutional repository IRUA

Electronic properties of 2H-stacking bilayer MoS_2 measured by terahertz time-domain spectroscopy

Xingjia Cheng,[1,2] Wen Xu*,[3,1,4,*] Hua Wen,[1,2] Jing Zhang,[1,2]
Heng Zhang,[1,2] Haowen Li,[3] and Francois M. Peeters[3,5]

[1] *Key Laboratory of Materials Physics, Institute of Solid State Physics, HFIPS, Chinese Academy of Sciences, Hefei 230031, China*

[2] *University of Science and Technology of China, Hefei 230026, China*

[3] *Micro Optical Instruments Inc., 518118 Shenzhen, China*

[4] *School of Physics and Astronomy and Yunnan Key Laboratory of Quantum Information of Yunnan Province, Yunnan University, Kunming 650091, China*

[5] *Department of Physics, University of Antwerp, Groenenborgerlaan 171, B-2020 Antwerpen, Belgium*

(Dated: September 28, 2022)

Abstract

Bilayer (BL) molybdenum disulfide (MoS_2) is one of the most important electronic structures not only in valleytronics but also in realizing twistronic systems on the basis of the topological mosaics in Moiré superlattices. In this work, BL MoS_2 on sapphire substrate with $2H$-stacking structure is fabricated. We apply the terahertz (THz) time-domain spectroscopy (TDS) for examining the basic optoelectronic properties of this kind of BL MoS_2. The optical conductivity of BL MoS_2 is obtained in temperature regime from 80 to 280 K. Through fitting the experimental data with the theoretical formula, the key sample parameters of BL MoS_2 can be determined, such as the electron density, the electronic relaxation time and the electronic localization factor. The temperature dependence of these parameters is examined and analyzed. Similar to monolayer (ML) MoS_2, BL MoS_2 with $2H$-stacking can respond strongly to THz radiation field and show semiconductor-like optoelectronic features. The theoretical calculations using density functional theory (DFT) can help us to further understand why the THz optoelectronic properties of BL MoS_2 differ from those observed for ML MoS_2. The results obtained from this study indicate that the THz TDS can be applied to study the optoelectronic properties of BL MoS_2 based twistronic systems for novel applications as optical and optoelectronic materials and devices.

PACS numbers:

*Electronic address: wenxu_issp@aliyun.com

I. INTRODUCTION

Since the discovery of graphene in 2004 [1], the investigation of atomically thin or two-dimensional (2D) electronic systems [2] has become one of the hot and fast-growing fields of research in condensed matter physics, material science, electronics and optoelectronics. At present, one of the most popularly studied 2D electronic systems is the few-layer and even monolayer (ML) transition metal dichalcogenides (TMDs) such as molybdenum disulfide (MoS_2) [3] and tungsten disulfide (WS_2) [4]. It has been found that the ML TMDs can exhibit the unique valleytronic properties which can be applied for, e.g., information storage and processing [5]. More interestingly, bilayer (BL) TMDs can be used to form the van der Waals (vdW) heterostructures in which topological mosaics in Moiré superlattices can be presented [6]. In such a case, the bilayer structures can offer an added layer degree of freedom. The interactions between two TMD layers with specific stacking order can significantly modify the electronic, optical [6] and vibrational properties of the electronic system. Thus, the twistronic features of the BL TMD system can be observed by tuning the vdW heterojunction from normal to the inverted type-II regime through, e.g., taking different stacking structures and/or applying an inter-layer bias voltage [6]. It is known that, similar to high-T_c superconductors, superconductivity can be observed in BL graphene based twistronic systems [7]. As for BL TMD based twistronic structures, novel electronic and optoelectronic phenomena, such as infrared inter-layer Moiré excitons [8], Dirac fermions with massive Dirac cones [9], on/off switching of the topological band inversion [6], etc, have been observed and studied. Therefore, it is important and significant to study the basic optoelectronic properties of the BL TMD systems, which becomes the prime motivation of the present research work.

In the present study, we focus our attention on one of the most popularly investigated BL TMD materials such as BL MoS_2. MoS_2 is a hexagonal crystal in which molybdenum is sandwiched between the sulfur atoms on both sides. Therefore, BL MoS_2 can have six types of the stacking structures [6] noted as H_X^X, H_M^M, H_X^M, R_X^M, R_M^X and R_M^M depending on the symmetry of the stacking configurations. Among them, H_X^M (or $2H$) is commonly formed BL stacking structure with a relatively high stacking symmetry. The other stacking configurations can be achieved by twisting and/or translating one of the MoS_2 layer away from $2H$-stacking. In contrast to gapless graphene, ML, BL and bulk MoS_2 have the energy

gaps between the conduction and valence bands, depending on the numbers and the stacking structures of the MoS_2 layers[10, 11]. The band gap E_g around the K-point decreases with increasing MoS_2 layers. It is found that $E_g \simeq 1.8$ eV, 1.6 eV and 1.29 eV for respectively ML, BL and bulk MoS_2[10–12]. Moreover, it is known that ML MoS_2 is with a direct band gap around the K-point[10]. In contrast, BL MoS_2 is with a weak direct band gap or even indirect band gap around the K-point, depending also on the stacking order. For $2H$-stacking BL MoS_2, the weak direct band gap can be presented around the K-point and the photoluminescence (PL) can be measured experimentally, although the PL efficiency of the BL MoS_2 is much lower in comparison to that of the ML MoS_2[10]. In addition, both ML and BL of MoS_2 show different degrees of band splitting at the top of the valence band around the K-point. For BL MoS_2, the effect of the band splitting is particularly pronounced for $2H$- and $3R$ (or R_X^M)-stacking configurations[13]. These features of the electronic band structures in ML, BL and bulk MoS_2 have been confirmed experimentally by the results obtained from, e.g., PL measurements[10, 14]. At present, the optical and optoelectronic properties of BL MoS_2 have been mainly studied in visible [15] and infrared [14] bandwidths, where the photon energy $\hbar\omega$ is larger than E_g, to look into mainly the effects of intra- and inter-layer excitons [6, 8]. Very recently, terahertz (THz) optoelectronic techniques have been applied for the investigation of BL MoS_2. The modulation of the optical conductivity of BL TMD heterojunctions was studied by varying the excitation optical power using light-pumped THz time-domain measurements [48]. The photovoltaic properties of BL TMD heterojunctions was studied by examining the delay between optical pumping and THz measurements [49]. We note that these investigations are based on the optical pump and THz probe (OPTP) technique in which the photon energy of pump radiation is larger than the energy gap of BL MoS_2. Therefore, these experimental work examined the optical response induced mainly by inter-band electronic transition accompanied by photon-generated carriers and associated exciton effect [48, 49]. The electronic relaxation time measured via OPTP normally corresponds to inter-band energy relaxation time.

In this work, we intend studying THz optoelectronic properties of BL MoS_2. Because THz photon energy is much smaller than the band gap of BL MoS_2 ($f = 1$ THz is about 4.13 meV), THz radiation normally does not cause the photon-induced carriers and associated intra- and inter-layer excitons in BL MoS_2. Thus, we can study the response of free-carriers in BL MoS_2 to the applied THz radiation field. In recent years, we have applied the tech-

nique of THz time-domain spectroscopy (TDS) for the investigation of optoelectronic[16] and magneto-optical[17] properties of ML MoS_2. In the present study, we would like to apply the similar technique to examine the electronic dynamics in BL MoS_2. Furthermore, because $2H$-stacking is the most basic BL structure for MoS_2 and for other BL TMD systems, here we would like to contribute a systematic experimental investigation into THz optoelectronic properties of $2H$-stacking BL MoS_2. Our aim of this study is at gaining an in-depth understanding of the basic physical properties of BL TMD materials for potential applications as advanced electronic and optoelectronic devices.

II. EXPERIMENT

A. Sample fabrication

In this study, BL MoS_2 on sapphire substrate was fabricated by using the standard technique of the chemical vapor deposition (CVD)[20–23]. MoO_3 (99.999% purity) and solid sulfur (99.999% purity) were applied as the molybdenum source and sulfur source, respectively, and argon was taken as the growth carrier gas. The sample growth was carried out in a dual temperature zone tube furnace with a diameter of 80 mm. The growth conditions were as follows: MoO_3 was heated to 650 °C, sulfur was heated to 180 °C, the growth pressure was at 4000 Pa, and the reaction time was 10 minutes. By using these growth conditions, the ML-MoS_2 on sapphire-wafer can be fabricated.

The slicing machine was used to cut the ML-MoS_2/sapphire-wafer into multiple 1×1 cm^2 square small sheets. Because the whole film is oriented, the orientation of every small film (s-film) is the same[18]. When we took each small piece of sample, we ensured that we operated without changing the original direction. The prepared ML MoS_2 small films (s-films) were peeled from sapphire square with the help of polydimethylsiloxane (PDMS) films. We attached the PDMS film to the surface of ML MoS_2 s-film, immersed the PDMS/MoS_2/sapphire-square in deionized water. Due to the difference in wettability between the MoS_2 and sapphire square surfaces, deionized water penetrated through the edges of the ML-MoS_2 and sapphire square to the interface between the two, thus being able to aid in the separation of the MoS_2 s-film from the sapphire square. So that we could slowly release the PDMS/MoS_2 s-film from the sapphire square. The first ML MoS_2 layer was

then transferred from combined ML-MoS_2/PDMS s-film onto another prepared sapphire substrate placed on a rotating stage by peeling off the PDMS film mechanically. Next, we used the rotating stage to rotate the first ML MoS_2 by 60° relative to the second ML MoS_2 layer. Then, the second PDMS/MoS_2 s-film was placed on the ML MoS_2/substrate and mechanically peeled off the PDMS film. As a result, one ML MoS_2 s-film can be transferred onto another ML MoS_2 on a substrate, with a twist angle of 60° between two layers. Before rotated the first layer, we had to make sure to align the two layers of MoS_2 s-films. This technique of sample growth and preparation is similar to those reported by other groups[18, 19]. It should be noted that due to the presence of the vdW force between two MoS_2 layers, $2H$-stacking type of the BL MoS_2 can normally obtained by using this technique.

The size of the BL MoS_2 sample used in this study is 1×1 cm^2 and the thickness of sapphire substrate is 0.3 mm. We note that the diameter of the THz light beam focused on the sample is about 3 mm in our experimental setup. Thus, the BL MoS_2 sample is big enough for the THz TDS measurement.

B. Sample characterization

We characterized experimentally the basic features of BL MoS_2 on sapphire by using atomic force microscope (AFM), Raman spectroscopy, and photoluminescence(PL). Figure 1(a) shows the results obtained from the measurement of the AFM on the sample. From AFM imaging, we can see that the MoS_2 film (lighter area) on sapphire substrate (darker area) is clean and smooth. By measuring the hight of the step-change between MoS_2 layer and the substrate along the line marked as white straight line in figure 1(a), we can determine the thickness of the MoS_2 film, which is about 1.3 nm. Because the thickness of ML MoS_2 is about 0.65 nm[21], the step-change of 1.3 nm in figure 1(b) suggests that the film is a BL MoS_2 structure[21, 22].

Figure 1(b) shows the Raman spectrum of BL MoS_2 on sapphire substrate using a 532 nm laser excitation at room-temperature. Two characteristic Raman peaks can be measured, which correspond respectively to in-plane Raman mode E^1_{2g} and out-of-plane Raman model A_{1g}[22]. The wave number difference of the two peaks, A_{1g}-E^1_{2g}, is about 22.1 cm^{-1}, in consistent with the result obtained for BL MoS_2[21, 22]. Moreover, by carefully analyzing the Raman spectrum via two Gaussian fittings (red and green curves), a peak “a” at about

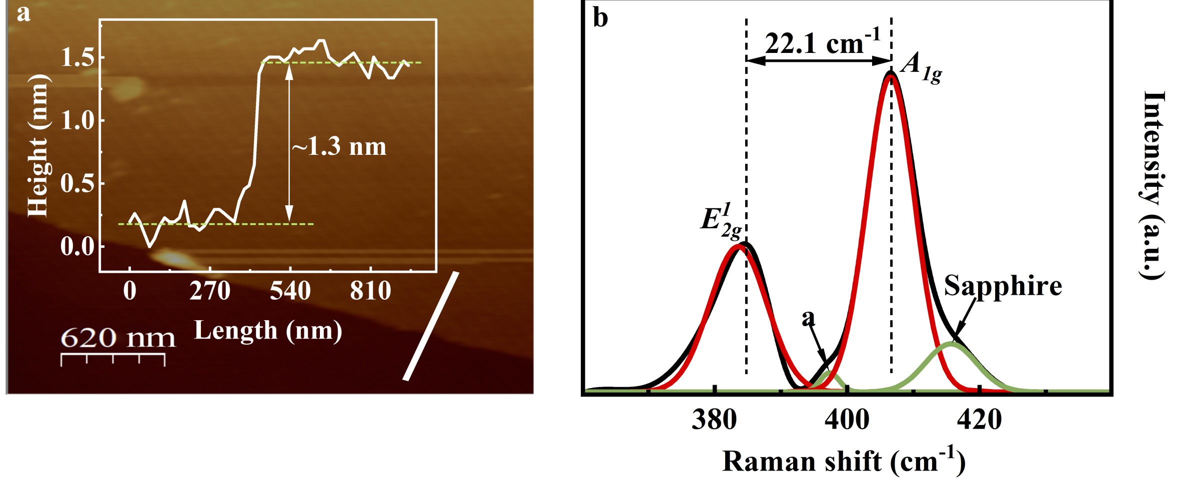

FIG. 1: (a) AFM image of BL MoS_2 on sapphire substrate. The inset shows the hight of the step-change between MoS_2 layer and the substrate along the line marked as white straight line, which corresponds to the thickness of the bilayer MoS_2. (b) Raman spectra of BL MoS_2 on sapphire substrate (black curve), measured at room-temperature by a 532 nm laser excitation. Two characteristic peaks for BL MoS_2, A_{1g} and E^1_{2g} with a spacing about 22.1 cm^{-1}, can be clearly identified. By spectral decomposition (red and green curves), the Raman peaks A_{1g} and E^1_{2g} along with "a" peak induced characteristically by the $2H$-stacking type and the characteristic peak for sapphire can be found.

396 cm^{-1} can be found, which corresponds to $2H$-stacking BL MoS_2[14]. The peak at ~ 417 cm^{-1} is the characteristic Raman peak of the sapphire substrate[22].

We apply a He-Ne laser (532 nm) as the light excitation source for the PL measurement at room temperature, with a grating of 1800 I/mm and the exposure time of 10 s. The signal reception is charge-coupled device (CCD) detector. The PL spectra for ML and BL MoS_2 on sapphire substrate and for sapphire substrate alone are measured respectively. The results shown in figure 2(a) are obtained by deducting the PL spectrum of the substrate from that for ML or BL MoS_2/substrate. In doing so, we are able to see more clearly those two PL peaks for $2H$-stacking BL MoS_2. The PL spectrum of BL MoS_2 on sapphire substrate (green curve) is shown in figure 2(a). For comparison, we also present the result for ML MoS_2 on sapphire substrate (blue curve) prepared by using the similar CVD technique[21–23]. The PL measurements were carried out at room temperature by using 532 nm laser excitation.

Two PL peaks, A at $\sim$1.86 eV and B at $\sim$2.01 eV, can be observed. These two peaks

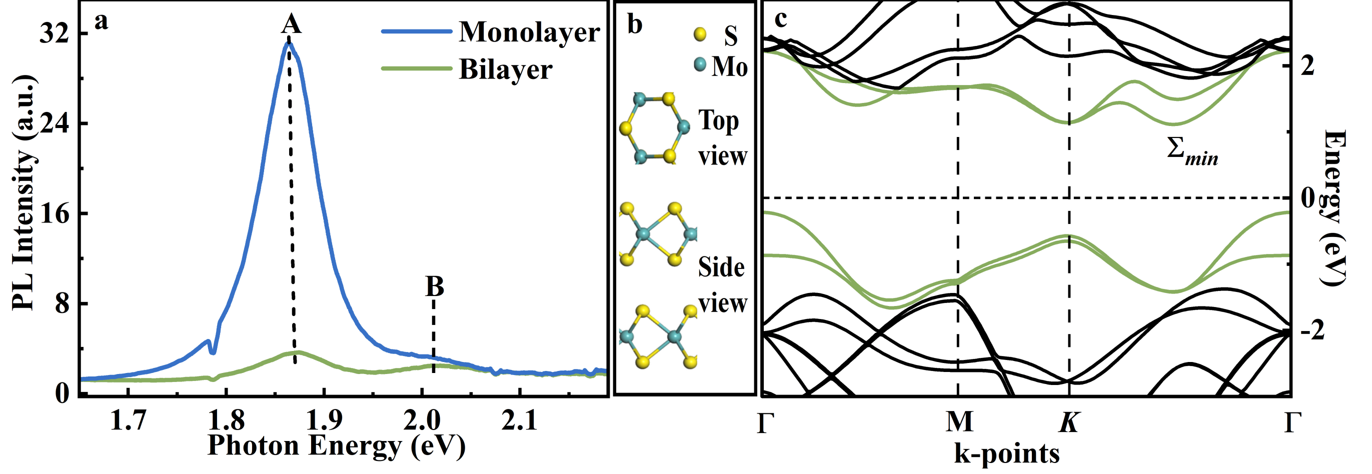

FIG. 2: (a) Photoluminescence (PL) spectra of ML (blue curve) and BL (green curve) MoS_2, measured at room-temperature using a 532 nm laser excitation, where the results are shown after deducting the signals from sapphire substrate. (b) Top and side views of the lattice structure of the $2H$-stacking BL MoS_2. (c) Electronic energy band structure of $2H$-stacking BL MoS_2, obtained from the DFT calculation. Here the Σ_{min}-point in the conduction band is lower than that in the K-point, with a difference about 27 meV.

are induced by excitonic transitions from split valence bands to the conduction band around the K-point in ML and BL MoS_2 (figure 2(c)). These results agree with those reported previously by other groups[15, 24]. As can be expected, the intensity of PL emission from BL MoS_2 is significantly weaker than that from ML MoS_2. These results can be further understood with the help of the electronic band structure (figure 2(c)) of $2H$-stacking BL MoS_2 structure (figure 2(b)), obtained from first principle calculation on the basis of DFT [25].

From above mentioned experimental measurements and findings, we can confirm that the sample used in this study is BL MoS_2 with $2H$-stacking configuration. Furthermore, the BL MoS_2 sample used in this study is n-type, confirmed by Hall measurement. It has been shown that BL MoS_2 with other stacking orders can also be grown by using the CVD technique[21–24].

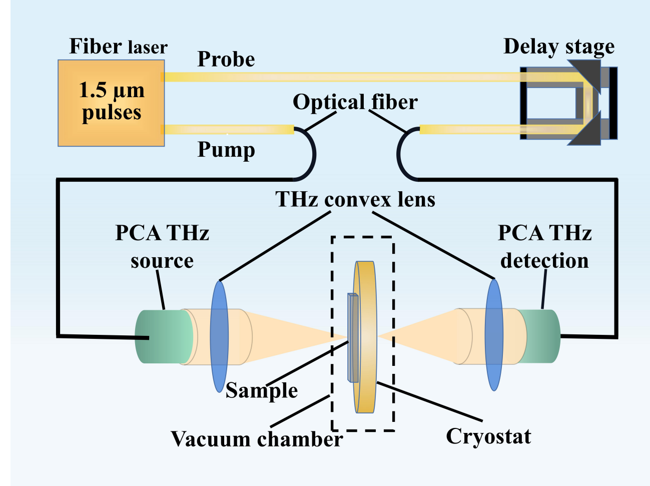

FIG. 3: Schematic diagram of the THz TDS system for optical transmission measurement. Here PCA is the photoconductance antenna.

C. Setup of THz time-domain spectroscopy

The schematic diagram of the THz TDS system used in this study is shown in figure 3. i) The pumping light source is a femtosecond (fs) fiber laser (ROI optoelectronics) with 1550 nm wavelength, 80 fs pulse width and 100 MHz repetition frequency. ii) The fs laser is divided into two beams. The higher intensity beam is the pump light, which irradiates on an InGaAs photoconductance antenna (PCA. Melno, Germany) to generate THz pulses. The lower intensity fs laser beam irradiates, with a time delay, on another InGaAs PCA for the detection of THz transmission through the sample via photo-electric sampling. iii) The generated THz beam is a horizontally polarized field, which is directed towards the sample surface normally. And iv) the sample is fixed on a sample holder in the cryostat (ST-500, Jains) with a quartz window, and the sample chamber is in a vacuum. Since the cryostat has a quartz window and quartz can only transmit efficiently up to 1.2 THz[27, 28], in the measurement we used the effective THz frequency ranging from 0.2 THz to 1.2 THz. In the present study, the variation of the temperature was down to liquid nitrogen temperature at about 80 K. Thus, we were able to measure the strength of the THz electric field transmitted through the sample as a function of the delay time in a temperature range from 80 K to 280 K. Moreover, the experimental system was slowly flushed with dry nitrogen gas to prevent the absorption of the THz waves by moisture and dusts in free-space.

III. THEORETICAL CALCULATION

By taking the lattice structure of $2H$-stacking BL MoS_2 as shown in figure 2(b), we study the corresponding electronic band structure via the DFT calculation as implemented in the VASP code using projector augmented wave pseudo-potentials and plane-wave expansions with a cut-off energy of 500 eV. In the calculation, the lattice parameter $a = 3.161$ Å, the Mo-Mo inter-layer distance $d = 6.147$ Å, and the Mo-S interatomic distance $l = 1.584$ Å along the [0001] direction of a relaxed $2H$-stacking BL MoS_2 crystal are taken in line with the corresponding experimental values[26]. A K-point mesh of $15 \times 15 \times 1$ in the first Brillouin zone is found to yield well-converged results. A vacuum space thickness of 20 Å is used to prevent any interactions between the adjacent periodic images of the BL structure. The atomic positions are optimized until all components of the forces on each atom are reduced to the values below 0.001 eV/Å. The exchange-correlation functional is treated within the Perdew-Burke-Ernzerhof (PBE) generalized gradient approximations (GGA). The electronic energy spectrum of $2H$-stacking BL MoS_2 obtained from this calculation is shown in figure 2(c). The detailed discussions of the electronic band structure of $2H$-stacking BL MoS_2 are presented in the section of Discussions.

IV. RESULTS AND DISCUSSIONS

A. THz transmission spectrum and optical conductivity

Applying transmission experiment based on THz TDS, we can measure the electric field strength transmitted through sapphire substrate $E_s(t)$ and through the sample (i.e., BL MoS_2 on substrate) $E_{ms}(t)$ in time-domain. In figure 4, we show $E_{ms}(t)$ measured at different temperatures. As can been seen (see inset in figure 4), $E_{ms}(t)$ depends sensitively on temperature. By Fourier transformation of $E_s(t)$ and $E_{ms}(t)$, we can obtain the corresponding electric field strength transmitted through sapphire substrate $E_s(\omega)$ and through the sample $E_{ms}(\omega)$ in frequency-domain, where $E_j(\omega) = |E_j(\omega)|e^{i\phi_j(\omega)}$. In figure 5, we show the modulus $|E_{ms}(\omega)|$ and the phase angle $\phi_{ms}(\omega)$ as a function of radiation frequency $f = \omega/2\pi$ for different temperatures. It is interesting to note that $|E_{ms}(\omega)|$ depends strongly on temperature, whereas $\phi_{ms}(\omega)$ shows a weak dependence upon temperature for BL MoS_2

on sapphire substrate.

From $E_s(\omega)$ and $E_{ms}(\omega)$, we can approximately evaluate the transmission coefficient for BL MoS_2 via[29]: $t_m(\omega) \simeq E_{ms}(\omega)/E_s(\omega)$, where the effect of the optical reflections from MoS_2 surface and from BL MoS_2/substrate interface are neglected[29]. It is known that optical conductivity, $\sigma(\omega)$, is a key and central physics quantity from which the optical coefficients such as absorption, transmission and reflection can be obtained by using the basic physics laws[30]. It is also a bridge quantity connecting optics and condensed matter physics. From $t_m(\omega)$ we can determine $\sigma(\omega)$ for BL MoS_2 via Tinkham formula[31]

$$t_m(\omega) = \frac{1 + N_s}{1 + N_s + Z_0\sigma(\omega)}, \quad (1)$$

where N_s is the index of refraction for the substrate, $N_s = 3.07$ for sapphire[21, 22], and $Z_0 \approx 377\ \Omega$ is the impedance of the free space. Because $t_m(\omega)$ is a complex quantity obtained via Fourier transformation, the optical conductivity is also a complex quantity $\sigma(\omega) = \sigma_1(\omega) + i\sigma_2(\omega)$. It is known that $\sigma_1(\omega)$ corresponds to the energy-consuming process or optical absorption, whereas $\sigma_2(\omega)$ describes the energy exchanging process between electrons and the radiation field. The real and imaginary parts of the optical conductivity for BL MoS_2 on sapphire are shown in figure 6 as a function of radiation frequency for different temperatures. The results obtained experimentally are shown by dotted curves. We find that with increasing radiation frequency $f = \omega/2\pi$, $\sigma_1(\omega)$ decreases in low-temperature regime 80 K $\leq T \leq$ 200 K and increases at relatively high-temperatures $T = 240$ K and 280 K. $\sigma_2(\omega)$ increases with ω in temperature regime from 80 K to 280 K. Both $\sigma_1(\omega)$ and $\sigma_2(\omega)$ increases with decreasing temperature.

B. Key sample parameters

From a view point of condensed matter physics and electronics, optical conductivity $\sigma(\omega)$ in an electronic material is mainly determined by electronic band structure, electronic scattering mechanisms such as impurities and phonons and by electron interactions with incident photons[32]. Because THz radiation does not cause photon-induced carriers in the electronic system, THz TDS measures mainly the electronic dynamics induced by free-carrier response to the radiation field. For a n-type BL MoS_2 sample, the optical conductivity is mainly determined by electronic transition within the conduction band. It is known that the

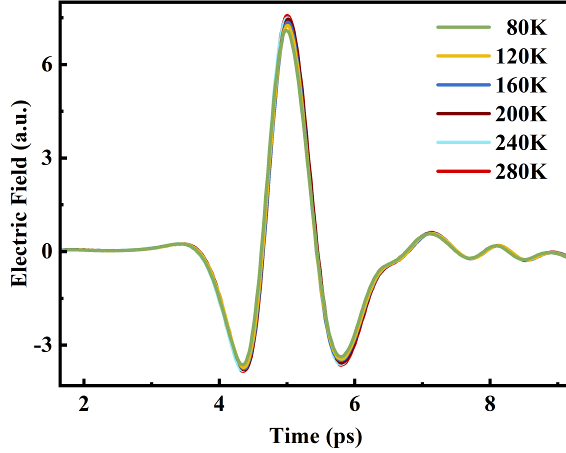

FIG. 4: Electric field strength $E_{ms}(t)$ of the THz beam transmitted through a BL MoS_2/sapphire sample as a function of delay time at different temperatures.

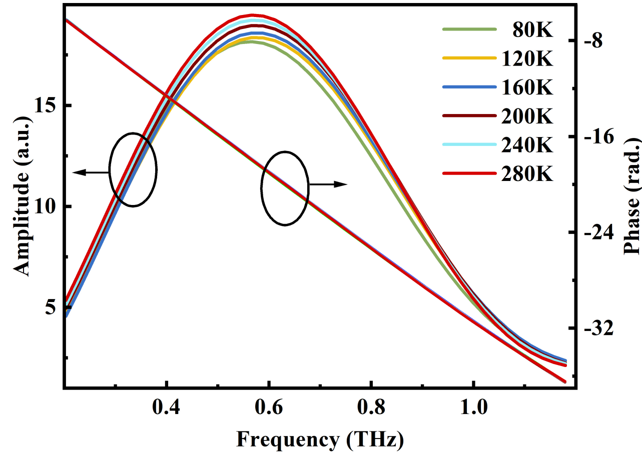

FIG. 5: Amplitude and phase angle of the THz electric field $E_{ms}(\omega)$ transmitted through a BL MoS_2-sapphire sample as a function of radiation frequency $f = \omega/2\pi$ at different temperatures.

commonly used theoretical approach to describe the optical conductivity for free-electrons is the Drude formula given as[33]

$$\sigma(\omega) = \frac{\sigma_0}{1 - i\omega\tau} = \frac{\sigma_0}{1 + (\omega\tau)^2} + i\frac{\sigma_0\omega\tau}{1 + (\omega\tau)^2}, \tag{2}$$

where $\sigma_0 = e^2 n_e \tau / m^*$ is direct current (DC) conductivity, n_e is the electron density in the system, τ is the electronic momentum relaxation time, and m^* is the effective electron mass. The Drude formula suggests that $\sigma_1(\omega)$ should decrease with increasing ω and $\sigma_2(\omega)$ should first increase then decrease with increasing ω. As shown in figure 6, both $\sigma_1(\omega)$ and $\sigma_2(\omega)$

obtained experimentally for BL MoS_2 on sapphire substrate do not obey the conventional Drude formula. In this study, we employ the Drude-Smith formula[34] for the understanding of our experimental results. By taking only the first collision term in the general Drude-Smith formula[34, 35] into consideration, the Drude-Smith formula can be written as

$$\sigma(\omega) = \frac{\sigma_0}{1 - i\omega\tau}(1 + \frac{c}{1 - i\omega\tau}), \tag{3}$$

where $c = [-1, 0]$ refers to the fraction of original velocity for an electron after a collision event, which corresponds to the effect of photon-induced electronic backscattering or localization[34]. We find that both $\sigma_1(\omega)$ and $\sigma_2(\omega)$ given by Drude-Smith formula can fit very well to those obtained experimentally, as shown in figure 6 (see solid curves). Through fitting the experimental data with the theoretical formula, we can obtain the DC conductivity σ_0, the electronic relaxation time τ and the electronic localization factor c for BL MoS_2. Moreover, it should be noted that in contrast to ML MoS_2 in which the conduction band minima is at the K-point, the bottom of the conduction band in $2H$-stacking BL MoS_2 is at the Σ_{min}-point (also see figure 2(c)). By taking the effective electron mass for $2H$-stacking BL MoS_2 as[36] $m^* \simeq 0.55m_e$, with m_e being the rest electron mass, we can get the electron density n_e in BL MoS_2 through the results obtained experimentally for σ_0. In figure 7 we show the electron density n_e, the electronic relaxation time τ and the electronic localization factor c as a function of temperature for BL MoS_2. As can be seen, i) n_e depends rather weakly on temperature in the regime from 80 K to 280 K, in line with experimental results reported by other research groups[37]; ii) τ decreases with increasing temperature, which is a typical feature of a semiconductor[31], and iii) $|c|$ increases with temperature, implying that the photon-induced electronic backscattering or localization increases with temperature.

Since BL MoS_2 is a semiconductor-like material, the electron-impurity and electron-phonon interactions are major channels for electronic scattering in the material. In the present study, we take a simple formula:

$$\frac{1}{\tau} = \frac{1}{\tau_I} + \alpha_{AC}T + N_0\Gamma_{LO}, \tag{4}$$

to fit the temperature dependence of the electronic relaxation time[38, 39] for BL MoS_2. Here, i) the first term $1/\tau_I$ is induced by electron-impurity scattering, which depends weakly on temperature[39]; ii) the second term $\alpha_{AC}T$ comes from electron interaction with acoustic-phonons, which depend normally linearly on temperature[38]; iii) the third term

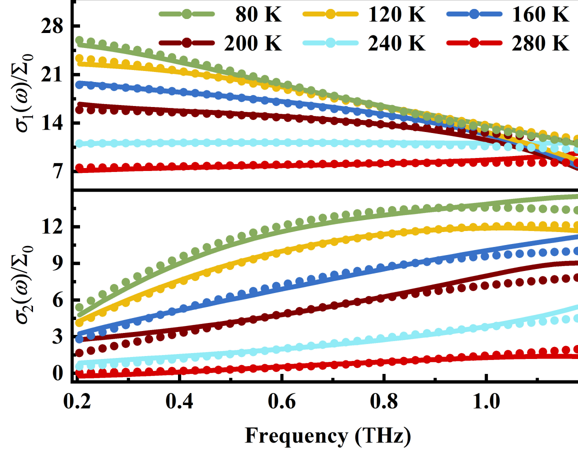

FIG. 6: Real $\sigma_1(\omega)$ (upper panel) and imaginary $\sigma_2(\omega)$ (lower panel) parts of the optical conductivity for BL MoS_2 as a function of radiation frequency $f = \omega/2\pi$ at different temperature. The dots are experimental results and the curves are obtained from Drude-Smith formula given by equation (3). Here $\Sigma_0 = e^2/4\hbar = 6.07 \times 10^{-5}$ S.

$N_0\Gamma_{LO}$ is attributed from electron coupling with longitudinal-optical (LO) phonons, where the temperature dependence of the scattering strength comes mainly from phonon occupation number[39] $N_0 = [e^{\hbar\omega_{LO}/k_BT} - 1]^{-1}$ with $\hbar\omega_{LO}$ being the LO-phonon energy. For BL MoS_2, $\hbar\omega_{LO} \approx 49$ meV, which is obtained from the "a" peak in the Raman spectrum in figure 1(b) and is the same as that obtained from other studies[40]; and iv) $1/\tau_I$, α_{AC} and Γ_{LO} are temperature-independent fitting parameters, regarding to different scattering centers. By fitting (figure 7(c)), we obtain τ_I=198.76 fs, $\alpha_{AC} = 2.61 \times 10^{-2}$ fs^{-1}K^{-1}, and $\Gamma_{LO} = 8.07 \times 10^{-6}$ fs^{-1}.

C. Further discussions

Now we discuss the important and unique features of $2H$-stacking BL MoS_2 from a view point of physics. From the results obtained from our DFT calculation, as shown in figure 2(c), we notice the following points. i) In sharp contrast to ML MoS_2 in which the minima of the conduction band is at the K-point, the conduction band minima in $2H$-stacking BL MoS_2 is at Σ_{min}-point[25, 36] between the K- and Γ-point. An indirect band gap can be found around the Σ_{min}-point. We find that the energy difference between the K-point and

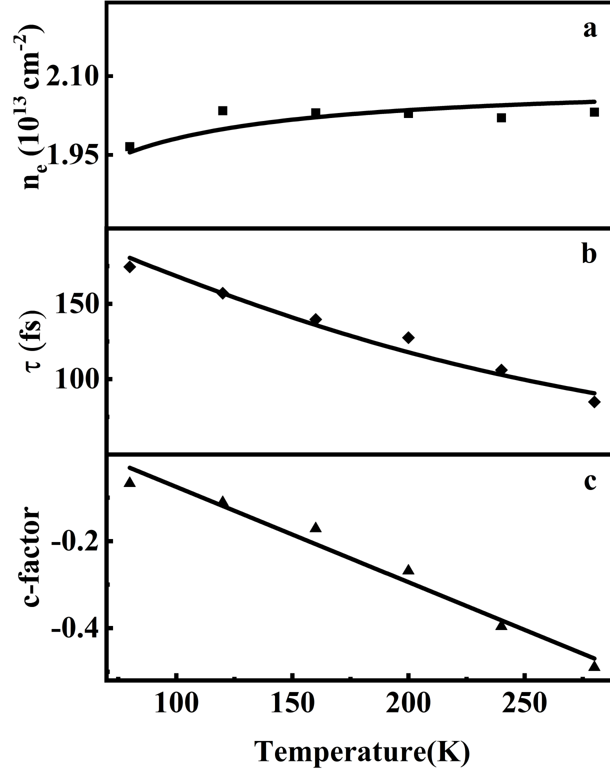

FIG. 7: Electron density n_e in a), electronic relaxation time τ in b), and electronic localization factor c in c), in $2H$-stacking BL MoS_2 as a function of temperature. In a) and c) the curves are drawn to guide the eye and in b) the curve is obtained by using equation (4).

Σ_{min}-point in the conduction band is about 27 meV. As a result, the electrons occupy mainly the states around the Σ_{min}-point in a n-type $2H$-stacking BL MoS_2. ii) In $2H$-stacking BL MoS_2, the top of the valence band at the Γ-point is markedly higher than that at the K-point, which also differs sharply from ML MoS_2 in which the valence band maxima is at the K-point. Thus, the holes occupy mainly the states around the Γ-point in a p-type $2H$-stacking BL MoS_2. However, an indirect band gap is presented around the Γ-point in $2H$-stacking BL MoS_2. And iii) the features of the direct band gap around the K-point is relatively weak for $2H$-stacking MoS_2. These characteristics are the main reasons why the photon-induced light generation from $2H$-stacking BL MoS_2 is significantly weaker than that from ML MoS_2, due to the presence of electronic transition channels accompanied by photon emission via indirect electron-photon coupling. As for PL emission from $2H$-stacking BL MoS_2 via excitonic effect, it can only occur around the K-point because the direct electron-

photon interaction normally does not vary the electronic momentum [41, 42], so that the inter-valley electronic transition is greatly impossible. Furthermore, for $2H$-stacking BL MoS_2, two conduction bands around the K-point are roughly degenerated, whereas the valance bands are split. This is the reason why two PL peaks can be observed for $2H$-stacking BL MoS_2 as shown in figure 2(a). It is known that the splitting of the valence band also occurs in ML MoS_2 [24] and in $3R$-stacking BL MoS_2[24]. Therefore, the B-peak marked in figure 2(a) can be observed not only in $2H$-stacking but also in ML and $3R$-stacking BL MoS_2[24]. However, the characteristic Raman peak "a" can help us to judge whether the BL structure is the $2H$-stacking or the $3R$-stacking[14].

After analyzing the calculation results of electronic band structure and the experimental results of PL test, we believe that the calculation results of energy band of $2H$-stacking BL MoS_2 are credible. Based on the results of the electronic band structure, we can also evaluate the effective electron mass m^* in the conduction band around the Σ_{min}-point in $2H$-stacking BL MoS_2, by fitting the band energy obtained from the DFT calculation with the energy spectrum $\hbar^2 k^2/(2m^*)$. In this work, we use $m^* = 0.55 m_e$ [36] to analysis the experimental results obtained from THz TDS measurement.

In a n-type $2H$-stacking BL MoS_2, the conducting electrons occupy mainly the states around the Σ_{min}-point. Thus, in contrast to the PL emission, the electronic transition induced by THz irradiation is achieved mainly via intra-band channel around the Σ_{min}-point. The conduction band in low-energy regime around the Σ_{min}-point, shown in figure 2(c) for $2H$-stacking BL MoS_2, is very much parabolic. As a result, the THz optoelectronic properties of a n-type $2H$-stacking BL MoS_2 are semiconductor-like so that the theory of the optical conductivity for free-electrons can be applied to describe the features of the THz response in n-type $2H$-stacking BL MoS_2. This is why we can use equation (4) for a semiconductor to fit the temperature dependence of electronic relaxation time τ in BL MoS_2. We note that τ in $2H$-stacking BL MoS_2 on sapphire substrate does not differ largely from that in ML MoS_2 on the same substrate[16]. Similar to conventional semiconductors, τ in $2H$-stacking BL MoS_2 decreases with increasing temperature (figure 7(c)). This is owing to the fact that the strength of electron interaction with acoustic phonons increases and the strength of electron−LO-phonon coupling increases with temperature because the phonon occupation number N_0 increases with temperature.

We find that the electron density n_e in a n-type $2H$-stacking BL MoS_2 on sapphire

substrate (figure 7(a)) is much higher than that in ML MoS_2[16]. This is mainly because of a bilayer structure with inter-layer vdW interaction and interaction between MoS_2 layers with the substrate. In comparison to ML MoS_2 on sapphire substrate where n_e increases significantly with increasing temperature, n_e in $2H$-stacking BL MoS_2 depends weakly on temperature. This implies that the donors in the BL-MoS_2/substrate system are most likely all ionized so that the effect of thermal ionization of the donors in the system becomes weak. The weak temperature dependence of n_e in BL MoS_2 has also been observed through electronic transport measurements[37].

It should be noted that in temperature regime from 80 to 300 K, the K-point in conduction band of $2H$-stacking BL MoS_2 may become occupied, so that two conducting channels from two valleys may contribute to THz conductivity. However, since the energy difference between the K-point and the Σ_{min}-point is about 27 meV obtained from our DFT calculation, the conducting electrons are largely populated in the Σ_{min}-band in $2H$-stacking BL MoS_2. Furthermore, the effective electron mass in Σ_{min}-point is heavier than that in K-point[43, 44]. The electronic density-of-states (DoS) in the Σ_{min}-band are therefore larger than those in the K-band because the DoS is proportional to m^* in a 2D electron gas system[25]. Consequently, the contribution to $\sigma(\omega)$ from electronic transition in the K-band is very small so that we can employ the theoretical model for single transition channel for the analysis and fitting of the experimental results.

Moreover, we found that the presence of the dielectric substrate can induce the electronic backscattering or localization effect in ML TMD systems[16, 45]. As shown in figure 6, this effect can also be observed in BL MoS_2, where the complex optical conductivity satisfies largely the Drude-Smith formula. When BL MoS_2 is placed on the substrate, charged impurities and phonons in the substrate can provide the additional scattering centers for electrons in BL MoS_2. This effect has been investigated in the graphene-based device[46, 47]. These additional scattering centers can further randomize the time dependence of the momentum and energy distribution of the electrons in BL MoS_2. Thus, the effect of electronic backscattering or localization can be enhanced by the presence of the substrate. Because the scattering rate increases with temperature, the effect of substrate-induced electronic localization also increases in BL MoS_2 on sapphire substrate (see figure 7(c)), noting that c is with a negative value).

V. CONCLUSIONS

In this study, we have fabricated the $2H$-stacking BL MoS_2 on sapphire substrate using the standard CVD technique. The THz TDS has been applied to measure the optoelectronic properties of this TMD based BL system. The theoretical calculation on the basis of the DFT theory has been carried out for understanding of the experimental findings. The main conclusions drawn from this work can be summarized as follows.

The electronic band structure in $2H$-stacking BL MoS_2 differs markedly from that in ML MoS_2. As a result, the weak PL emission from $2H$-stacking BL MoS_2 is mainly induced by exciton effect occurring around the K-point, whereas the THz response is mainly achieved through intra-band electronic transition accompanied by the absorption of photons around the Σ_{min}-point which is in-between the K- and Γ-point in $2H$-stacking BL MoS_2.

Through THz TDS measurement, we can obtain the complex optical conductivity for $2H$-stacking BL MoS_2. It is found that $\sigma(\omega)$ for $2H$-stacking BL MoS_2 sapphire substrate does not obey the conventional Drude formula for optical conductivity. But it can be reproduced by the Drude-Smith formula in which the effect of photon-induced electronic backscattering has been considered. By fitting the experimental results with the theoretical formula, we are able to determine optically the key sample parameters in BL MoS_2, such as the electron density, the electronic relaxation time, and the electronic localization factor. The temperature dependence of these parameters has been examined. It has been found that the THz optoelectronic properties of $2H$-stacking BL MoS_2 are semiconductor-like, where the electron density depends weakly on temperature in 80 K to 300 K regime and the electronic relaxation time decreases with increasing temperature owing to the presence of electron-phonon scattering. Furthermore, similar to ML MoS_2 on a dielectric substrate, the substrate-induced electronic backscattering or localization can also be observed in BL MoS_2 on sapphire substrate. It should be noticed that by using THz TDS, we do not need the external magnetic field for the determination of the electron density via, e.g., the Hall measurement.

$2H$-stacking BL MoS_2 is a basic structure in twistronic system. The other five stacking configurations can be achieved by twisting and/or translating one of the MoS_2 layer away from $2H$-stacking. Therefore, the investigation of $2H$-stacking BL MoS_2 is of great importance and significance for the understanding of TMD based BL twistronic systems. We

hope that the results obtained from this study can contribute an in-depth understanding of the basic optoelectronic properties of bilayer TMD materials and can be the basis for the application of BL MoS_2 in advanced optical and optoelectronic devices.

ACKNOWLEDGMENTS

This work was supported by the National Natural Science foundation of China (NSFC) (Grants No. U1930116 and No. U206720039) and by Shenzhen Science and Technology Program (No. KQTD20190929173954826).

---

[1] Novoselov K S, Geim A K, Morozov S V, Jiang D, Zhang Y, Dubonos S V, Grigorieva I V and Firsov A A 2004 Science **306** 666-669

[2] Castellani C, DiCastro C and Lee P A 1998 Phys. Rev. B **57** R9381-R9384

[3] Fai M K, Di X and Jie S 2018 Nat. Photonics **12** 451-460

[4] Hill H M, Rigosi A F, Roquelet C, Chernikov A and Heinz T F 2015 Nano Lett. **15** 2992-2997

[5] Xiao D, Liu G B, Feng W, Xu X and Yao W 2012 Phys. Rev. Lett. **108** 196802

[6] Tong Q J, Yu H, Zhu Q, Wang Y, Xu X and Wang Y 2017 Nat. Phys. **13** 356-362

[7] Cao Y, Fatemi V, Fang S, Watanabe K, Taniguchi T, Kaxiras E and Jarillo-Herrero P 2018 Nature **556** 43-50

[8] Seyler K, Rivera P, Yu H, Wilson N, Ray E, Mandrus D, Yan J, Yao W and Xu X 2019 Nature **567** 66-70

[9] Cai T, Yang S A, Li X, Zhang F, Shi J, Yao W and Niu Q 2013 Phys. Rev. B **88** 115140

[10] Mak K F, Lee C, Hone J, Shan J and Heinz T F 2010 Phys. Rev. Lett. **105** 136805

[11] Lee C G, Yan H G, Louis E B, Tony F H, James H and Sunmin R 2010 ACS Nano **4** 2695-2700

[12] Padilha J E, Peelaers H, Janotti A and Van C G 2014 Phys. Rev. B **90** 205420

[13] Zhang X Z, Zhang R Y, Zhang Y, Jiang T, Deng C Y, Zhang X A and Qin S Q 2019 Opt. Mater. **94** 213-216

[14] Xia M, Li B, Yin K, Capellini G and Xie Y H 2015 ACS Nano **9** 12246-12254

[15] Van A M, Kunstmann J, Chernikov A, Chenet D A, You Y M, Zhang X X, Huang P Y, Berkelbach T C, Wang L and Zhang F 2014 Nano Lett. **14** 3869-3875

[16] Wang C, Xu W, Mei H, Qin H, Zhao X, Zhang C, Yuan H F, Zhang J, Xu Y, Li P and Li M 2019 Opt. Lett. **44** 2139-2142

[17] Wen H, Xu W, Wang C, Song D, Mei H Y, Zhang J and Ding L 2020 Nano Select **2** 90-92

[18] Liao M, Wei Z, Du L, Wang Q Q, Jiang T, Yu H, Wu F, Zhao J J, Xu X and Han B 2020 Nat. Commun. **11** 2153

[19] Yu H, Liao M Z, Zhao W J, Liu G D and Zhang G Y 2017 ACS Nano **11** 12001-12007

[20] Yu Y, Li C, Liu Y, Su L, Zhang Y and Cao L 2013 Sci. Rep. **3** 1866

[21] Wang X, Feng H, Wu Y and Jiao L 2013 J. Am. Chem. Soc. **135** 5304-5307

[22] Sajjad H, Muhmmad A S, Dhanasekaran V, Muhmmad Z I, Jai S, Muhmmad F K, Jonghwa E, Yongho S and Jongwan J 2015 J. Alloy. Compd. **653** 369-378

[23] Zhu C R, Wang G, Liu B L, Marie X and Qiao X F 2013 Phys. Rev. B. **88** 121301

[24] Ullah F et al 2021 ACS Appl. Mater. &Inter. **13** 57588-57596

[25] Ellis J K, Lucero M J and Scuseria G E 2011 Appl. Phys. Lett. **99** 261908

[26] Bhattacharyya S and Singh A K 2012 Phys. Rev. B **86** 075454

[27] Christiansen P L, Srensen M P and Scott A C 2000 *Nonlinear Science at the Dawn of the 21st Century*, Springer Berlin Heidelberg

[28] Hangyo M, Nagashima T and Nashima S 2002 Meas. Sci. Technol. **13** 1727

[29] Duvillaret L, Garet F and Coutaz J L 1996 IEEE J. Sel. Top. Quant. **2**, 739-746

[30] Nudelman S and Mitra S S 1969 *Optical Properties of Solids*, Springer

[31] Tinkham M 1956 Phys. Rev. B **104** 845

[32] Jackson J D 1998 *Classical Electrodynamics, 3rd Edition*, SWiley

[33] Drude P 1890 *Bestimmung der optischen Constanten der Metalle*, Annalen Der Physik

[34] Smith N V 2001 Phys. Rev. B **64** 155106

[35] Han F W, Xu W, Li L L and Zhang C 2016 J. Appl. Phys. **119** 245706

[36] Mukhopadhyay A, Kanungo S and Rahaman H 2021 J. Computat. Electron. **20** 161-168

[37] Baugher B, Churchill H, Yang Y and Jarillo-Herrero P 2013 Nano Lett. **13** 4212-4216

[38] Valerini D, Cretí A, Lomascolo M, Manna L, Cingolani R and Anni M 2005 Phys. Rev. B **71** 235409

[39] Xu W, Peeters F M and Lu T C 2009 Phys. Rev. B **79** 037403

[40] Kim S et al 2012 Nat. commun. **3** 1011

[41] Schwarz H 1972 *Laser Interaction and Related Plasma Phenomena*, Springer US

[42] Xu W, Dong H M, Li L L, Yao J Q, Vasilopoulos P and Peeters F M 2010 Phys. Rev. B **82** 125304)

[43] Yun W S, Han S W, Hong S C, Kim I G and Lee J D 2012 Phys. Rev. B **85** 033305

[44] Scalise E and Houssa M and Pourtois G and Afanas V and Stesmans A 2014 Physica E **56** 416-421

[45] Dong H M, Tao Z H, Li L L, Huang F, Xu W and Peeters F M 2020 Appl. Phys. Lett. **116** 203108

[46] Dong H M, Xu W, Zeng Z, Lu T C and Peeters F M 2008 Phys. Rev. B **77** 235402

[47] Zhang S H, Xu W, Badalyan S M and Peeters F M 2013 Phys. Rev. B **87** 075443

[48] Kumar S, Singh A, Kumar S, Nivedan A, Tondusson M, Degert J, Oberle J, Yun S J, Lee Y H and Freysz E 2021 Opt. Express **87** 4181-4190

[49] Bala Murali Krishna M, Mado J, Urquizo J P, Zhu X, Vinod S Shekar Tiwary C, Ajayan M P and Dani M K 2018 Semicond. Sci. Technol. **33** 084001